[4]J. L. Lebowitz and A. Martin-Löf, Commun. Math. Phys. (to be published).
[5]R. B. Griffiths (private communication).
[6]F. J. Dyson, Commun. Math. Phys. 12, 91 (1969); 21, 269 (1971).
[7]See, for example, M. E. Fisher, Rept. Progr. Phys. 30, 615 (1967); or M. E. Stanley, *Introduction to Phase Transitions and Critical Phenomena* (Oxford U. P., London, 1971).
[8]J. Stephenson, J. Chem. Phys. 54, 890 (1971). The inequality was also derived by Stephenson for more general fluid systems using some assumptions on the continuity of the slopes of the isochares at β_c.
[9]R. B. Griffiths, C. A. Hurst, and S. Sherman, J. Math. Phys. 11, 790 (1970).
[10]J. L. Lebowitz, Phys. Letters 33A, 99 (1971).

PHYSICAL REVIEW B VOLUME 5, NUMBER 7 1 APRIL 1972

Structural Aspects of the Metal-Insulator Transitions in Cr-Doped VO_2

M. Marezio, D. B. McWhan, J. P. Remeika, and P. D. Dernier
Bell Telephone Laboratories, Murray Hill, New Jersey 07974
(Received 8 September 1971)

The temperature-composition phase diagram of $V_{1-x}Cr_xO_2$ with $0 \leq x \leq 0.025$ is found to contain four phases: rutile (R), normal monoclinic VO_2 (M_1), and two monoclinic phases (M_2 and M_3). For M_2 with $x = 0.024$ at 298 °K, $2a_R \approx a_M = 9.0664$, $2c_R \approx b_M = 5.7970$, $a_R \approx c_M = 4.5255$ Å, and $\beta = 91.88°$. The M_2 and M_3 regions are separated by a volume discontinuity. There are two types of V atoms in these structures. The first type form pairs and the second type form zig-zag chains along the b_M axis. This contrasts with VO_2 where all the vanadium atoms are paired. The structures R, M_2, and M_3 with $x = 0.024$ have been refined from single-crystal x-ray data. High-pressure resistivity and x-ray measurements vs temperature give $dT(M_2 \rightarrow R)/dP = -(0.9 \pm 0.1)$ °K/kbar and $V_R - V_{M_2} = -0.11$ cm^3/mole VO_2. At higher pressures $dT(M_3 \rightarrow R)/dP = (0 \pm 0.2)$ °K/kbar. These results cannot be simply interpreted in terms of the homopolar bond model proposed for the M_1 phase of VO_2.

I. INTRODUCTION

Many of the vanadium oxides exhibit temperature-induced metal-insulator transitions.[1,2] Those in V_2O_3 and the Magnéli phases V_nO_{2n-1} $(4 \leq n < 8)$ are distinguished from the transition in VO_2 as only in the latter is there no antiferromagnetic phase. Recent studies of V_2O_3 doped with Cr and Ti have led to a generalized phase diagram for the sesquioxides[3,4] and this diagram has been interpreted in terms of a Mott transition from itinerant-to-localized-electron states.[3] The experiments reported in the literature on doped VO_2 indicate that this transition is quite different. The addition of Ti,[5,6] Cr,[7] Al,[7] or Fe[7] leads to phases at room temperature which have different structures from the normal monoclinic phase of pure VO_2. It is not clear if these different phases are related as they have been reported as having orthorhombic,[7] monoclinic,[5,6] or triclinic[8] symmetry by x-ray-diffraction methods.

Recently, Villeneuve *et al.* reported a phase diagram for the system $V_{1-x}Cr_xO_2$ which is based on magnetic susceptibility, electrical resistivity, and powder-x-ray-diffraction measurements.[9] They find on adding Cr a sequence of phases with increasing temperature of monoclinic to orthorhombic to tetragonal (rutile) with the insulator-to-metal transition being associated with the latter crystallographic transition. The metallic phase is more dense than the insulating phase, in contrast to pure VO_2 where the insulator is slightly more dense. This implies that the transition temperature of Cr-doped VO_2 will decrease with increasing pressure. As crystals of VO_2 doped with 2.4-at.% Cr were available from the earlier studies of MacChesney and Guggenheim,[10] a complete determination of the crystal structure of the intermediate phase was undertaken and measurements of the pressure dependence of the transition temperature were made. In the course of this work it became necessary to study the low-Cr-concentration region in more detail and this was done using ceramic samples.

This paper is divided into four parts. The temperature-composition phase diagram is given in Sec. II and the temperature-pressure diagram for crystals of VO_2 + 2.4-at.% Cr in Sec. III. The crystal structure is given in Sec. IV for three different temperatures corresponding to three different phases. Finally in Sec. V this work is related to current theories for the metal-insulator transitions in VO_2.

II. TEMPERATURE-COMPOSITION PHASE DIAGRAM

The phase diagram was determined using both the single-crystal sample of $V_{0.976}Cr_{0.024}O_2$ and ceramic samples made in different ways. The sequence of

phases with temperature was the same for all the samples, but the exact position of the different phase boundaries is uncertain because the transitions are very sensitive to the Cr concentration and the oxygen stoichiometry. Ceramic samples of $V_{1-x}Cr_xO_2$ were made from appropriate mixtures of V_2O_3, V_2O_5, and Cr_2O_3. In most of the samples the mixtures were ball milled in ethyl alcohol using Al_2O_3 balls for 16 h and then were immediately vacuum filtered. The resulting mixture was pressed into a pellet and heated in a platinum boat under purified nitrogen at 1000 °C for 16 h. Samples were made at ten different compositions between $x = 0.00$ and $x = 0.025$. Powder-x-ray-diffraction patterns revealed a clean transition from the normal monoclinic structure of pure VO_2 (M_1)[11] to a second monoclinic structure (M_2) described in Sec. IV. The transition occurred at approximately $x = 0.0035$. Some of the samples were reground in an agate mortar, ball milled, and fired as above. This moved the composition at which the transition occurs at room temperature to $x = 0.005$. It is not clear if the shift occurred because of better homogeneity in the sample or because of a change in oxygen stoichiometry.

Villeneuve *et al.* reported that the intermediate phase was orthorhombic, contrary to the single-crystal results given in Sec. IV.[9] To see if this difference resulted from the method of sample preparation, samples of $V_{0.975}Cr_{0.025}O_2$ and $V_{0.9}Cr_{0.1}O_2$ were made in evacuated quartz tubes at 1300 °K, as described in Ref. 9. Also, to eliminate possible contamination by the Al_2O_3 balls and changes in oxygen stoichiometry, samples were prepared without ball milling and with ± 2-at. % V_2O_5 from the calculated amount. In all cases the monoclinic phase was found, but there were small changes in lattice parameters depending on the conditions and on refiring.

X-ray-diffraction measurements were made as a function of temperature using a Phillips diffractometer and filtered Cu radiation. The temperature was varied from 100 to 400 °K by blowing nitrogen gas of the appropriate temperature over the sample. Four distinct regions were found as a function of Cr concentration and temperature. At high temperatures the tetragonal rutile (R) structure was found at all compositions studied. At low temperatures and low Cr concentration the VO_2 monoclinic phase (M_1) was found. At higher Cr concentrations ($x = 0.025$) a different monoclinic phase M_2 was observed. However, an anomaly in the lattice parameters and volume occurred in the M_2 phase as a function of temperature. From the powder-x-ray-diffraction measurements it is not clear if this is a first-order transition with no change in structure as occurs in some of the Magnéli phases such as[12] Ti_4O_7 or whether it is only a region of anomalous change as in[13] Ti_2O_3 and not a transition in the thermodynamic sense. The pressure-temperature phase diagram described in Sec. III is more compatible with the existence of a first-order transition. The regions above and below the anomaly were designated M_2 and M_3, respectively. At intermediate compositions the sequence $R \rightarrow M_2 \rightarrow M_3 \rightarrow M_1$ was observed with decreasing temperature. Similar results were obtained from both single-crystal and ceramic samples. The resulting phase diagram for the refired samples is shown in Fig. 1. The different temperatures are known to ± 3 °K. The

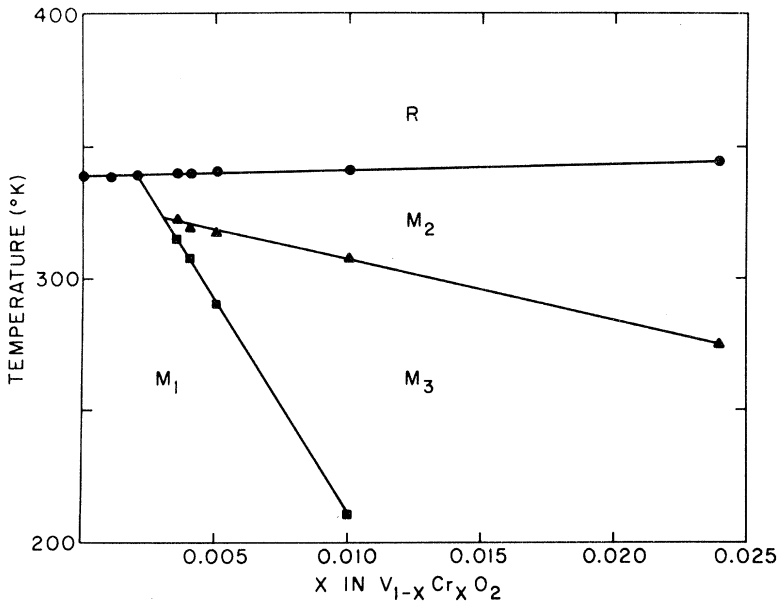

FIG. 1. Tentative temperature-composition phase diagram for $V_{1-x}Cr_xO_2$ as determined from powder-x-ray-diffraction measurements. R is rutile, M_1 is monoclinic phase observed in pure VO_2 (Ref. 11), M_2 and M_3 are intermediate monoclinic phases described in Sec. IV; the two phases are separated by an apparent discontinuity in volume but with no change in symmetry (Fig. 2). The M_3 phase extends to 5 °K for $x = 0.024$.

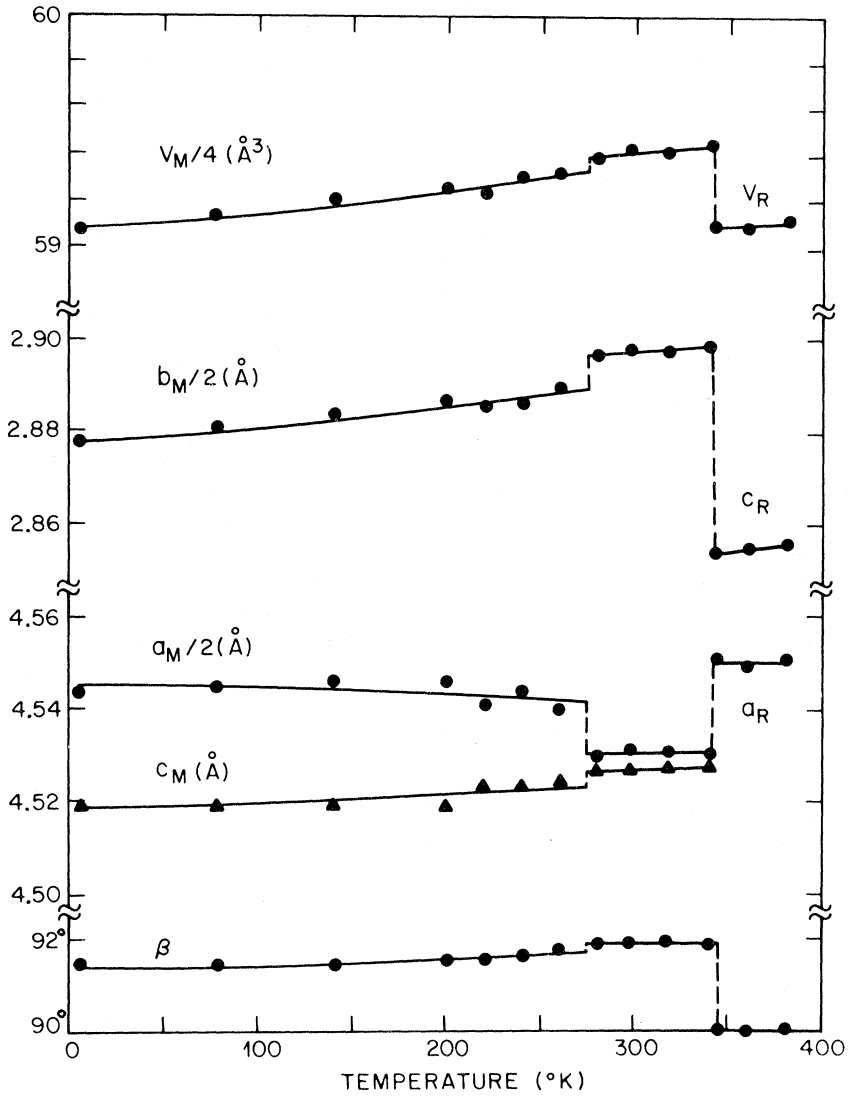

FIG. 2. Lattice parameters and volume vs temperature for $V_{0.976}Cr_{0.024}O_2$. Above ~345 °K the tetragonal rutile structure exists. Below 345 °K the structure is monoclinic. At ~275 °K there is a discontinuity in lattice parameters and volume with no change in symmetry.

lattice parameters and volume of a sample with $x = 0.024$ are shown as a function of temperature in Fig. 2. This sample did not show a transition to the M_1 phase down to liquid-helium temperatures. An anomaly in the magnetic susceptibility has been reported for $x = 0.025$ at ≈ 270 °K, and it was ascribed to a transition from M_1 to M_2.[9] The susceptibility of the single-crystal sample with $x = 0.024$ was measured and the results are shown in Fig. 3. An anomaly similar to that reported in the literature is observed but it is associated with the anomaly in lattice parameters shown in Fig. 2.

The transition from M_3 to M_1 must be first order. The powder pattern of the M_3 phase is such that it cannot be indexed on the M_1 unit cell or vice versa. Therefore, neither phase can be regarded as a simple distortion of the other. We wish to note, however, that the first strong pair of reflections in M_3 appear to coalesce smoothly with decreasing temperature instead of decreasing in intensity with the appearance of a central reflection corresponding to the M_1 phase. This behavior would indicate that at the transition the volumes of the two phases must be equal. The $\Delta 2\theta$ of $(110)_R \Rightarrow (\bar{2}01)$, $(201)_{M2,M3} \Rightarrow (011)_{M_1}$ and the unit cell volume as a function of temperature for a sample with $x = 0.01$ are shown in Fig. 4.

III. TEMPERATURE-PRESSURE PHASE DIAGRAM FOR VO_2 + 2.4-at.% Cr

The electrical resistivity of several samples was measured as a function of temperature and pressure using high-pressure equipment described earlier.[14,15] The pressure medium was AgCl and the pressure calibration is relative to the 25.4-kbar transition of a Bi wire mounted axially in the cell.

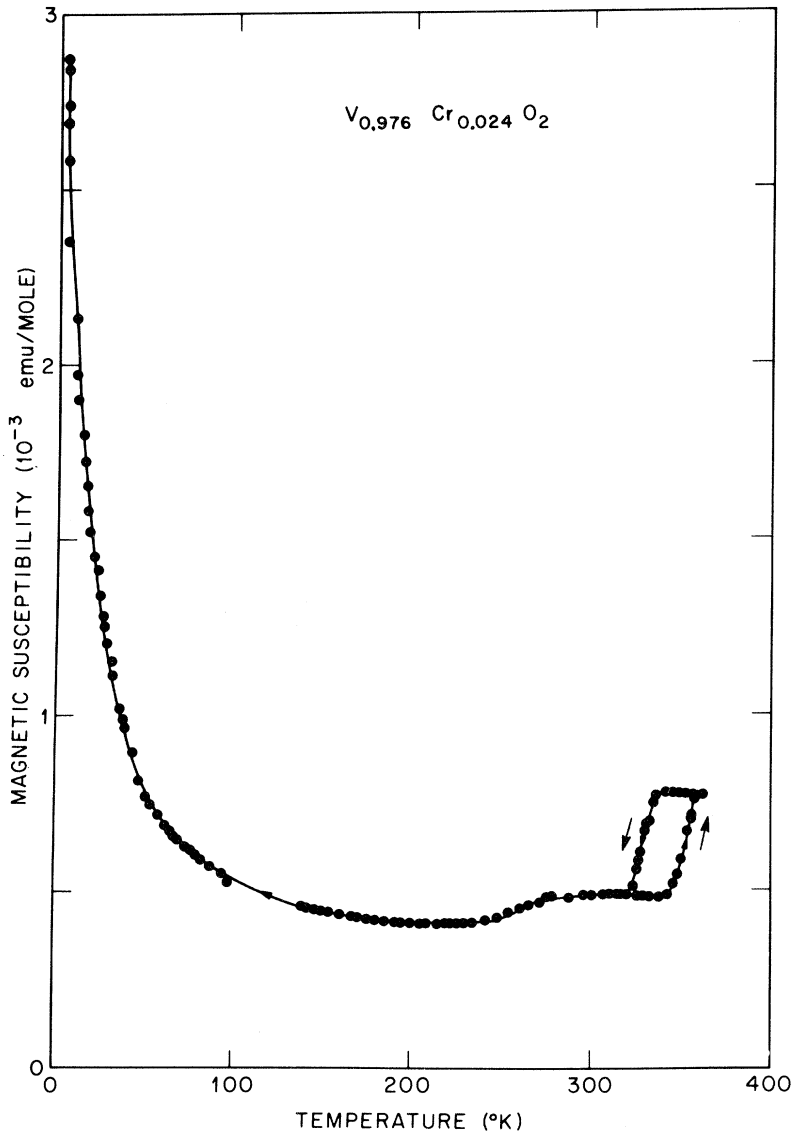

FIG. 3. Magnetic susceptibility vs temperature for a crystal of $V_{0.976}Cr_{0.024}O_2$. Note two transitions corresponding to those shown in Fig. 2. Low-temperature rise in susceptibility can be fitted by $\chi = 0.3 + 0.025/(T+3)$ (10^{-3} emu/mole). The resulting effective moment is less than expected for localized Cr^{3+} impurities.

The resistivity as a function of temperature is shown in Fig. 5 for three samples. The transition temperatures observed on warming are shown as a function of pressure in Fig. 6. The points are numbered to indicate the sequence of measuring the temperatures. The results are clearly reversible and appear to have a change in slope between 25 and 30 kbar. There is also a clear difference in the sharpness and hysteresis of the transition below and above this pressure range, as illustrated in the inset in Fig. 5. In the higher-pressure range the transition temperature is independent of pressure within experimental error (± 0.2 °K/kbar). This is similar to pure VO_2 where $dT/dP = +0.08$ °K/kbar.[16,17] At lower pressures $dT/dP = -(0.9 \pm 0.1)$ °K/kbar and using the volume change of $V_R - V_{M_2} = -0.11$ cm^3/mole VO_2, the Clapeyron equation gives an entropy change of $S_R - S_{M2} = 2.9 \pm 0.7$ e.u. This is comparable with that found in pure VO_2, 3.0 e.u.,[18] and indicates that the bulk of the entropy change is associated with the metal-insulator transition. The remaining part of the phase diagram has not been uniquely determined. The change in slope implies that a triple point exists. As M_3 is stable at 1 atm below 275 °K, it is reasonable to connect this point and the triple point. In fact, in two experiments a slight decrease in resistivity was observed at room temperature with increasing pressure at 9–14 kbar. A change in resistivity was not observed as a function of temperature. The assignment of the M_1-M_3 phase boundary can be checked by thermodynamics. There are experimental values for the three slopes (dP/dT) and two of the volume changes at 1 atm. The

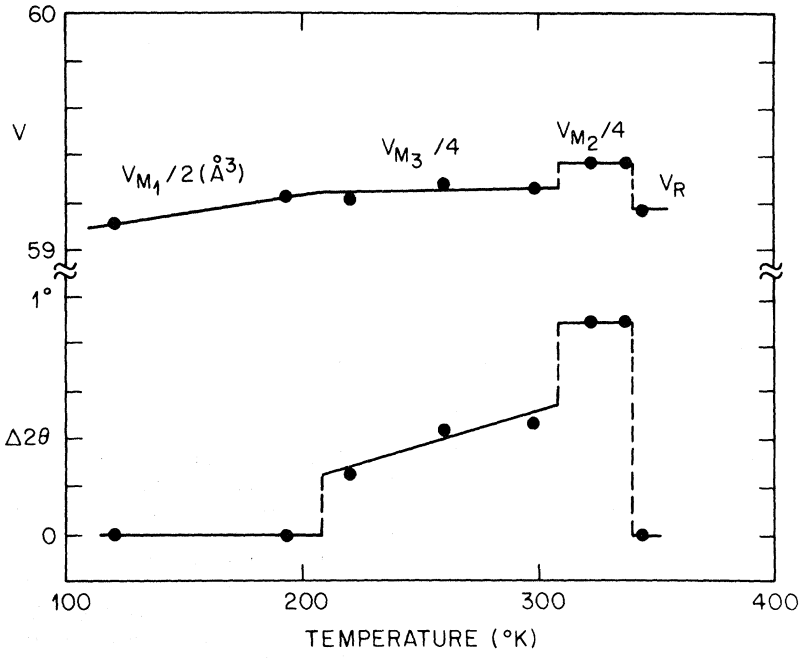

FIG. 4. Separation of the pseudorutile (110) reflection and unit-cell volume vs temperature for a ceramic sample of $V_{0.99}Cr_{0.01}O_2$. A set of distinct discontinuities occur which correspond to the sequence of structures $R \rightarrow M_2 \rightarrow M_3 \rightarrow M_1$ with decreasing temperature.

conservation of entropy and of volume around a triple point and the Clapeyron equation $dT/dP = \Delta V/\Delta S$ can be used with four of the experimental values to calculate the fifth value in order to see if it is consistent with the observed value. A calculation of dT/dP for the R-M_3 transition gives a range of $dT/dP = -(0.2\text{–}0.8)$ °K/kbar which is slightly larger than the observed value of (0 ± 0.2) °K/kbar. In view of the combined experimental errors this is probably a reasonable agreement.

IV. CRYSTAL STRUCTURE OF VO_2 + 2.4-at.% Cr

The single crystals of $V_{0.976}Cr_{0.024}O_2$ were obtained from a boule grown by MacChesney and Guggenheim.[10] Two small fragments were ground into spheres of 0.034- and 0.032-cm diam, respectively. Precission photographs taken at room temperature with Mo$K\alpha$ x rays showed extensive twinning. All principal diffraction spots could be indexed on the basis of a monoclinic cell related to the rutile cell by the following matrix equation:

$$\begin{pmatrix} a \\ b \\ c \end{pmatrix}_{M_2} = \begin{pmatrix} 2 & 0 & 0 \\ 0 & 0 & 2 \\ 0 & \bar{1} & 0 \end{pmatrix} \begin{pmatrix} a \\ b \\ c \end{pmatrix}_R .$$

All the satellite diffraction spots could be indexed assuming that the twinning elements were $4mm$, with the fourfold axis along the b_{M_2} axis. Upper-layer photographs clearly revealed that the true symmetry of this structure was indeed monoclinic. The only systematic absence among all the reflections was $h+k=2n+1$, which led to space group $C2/m$, with eight formulas per unit cell. Four vanadium atoms are in the special positions $4g$ $(0y0)$ and four in $4i$ $(x0z)$. Eight oxygen atoms are in the general positions while two sets of four are in the special positions $4i$ $(x0z)$. The monoclinic phase (M_1) of pure VO_2 has the space group $P2/c$ and its unit cell is obtained from the rutile cell by the matrix equation

$$\begin{pmatrix} a \\ b \\ c \end{pmatrix}_{M_1} = \begin{pmatrix} 0 & 0 & 2 \\ 1 & 0 & 0 \\ 0 & 1 & \bar{1} \end{pmatrix} \begin{pmatrix} a \\ b \\ c \end{pmatrix}_R .$$

In Table I the observed and calculated d spacings are reported. The powder pattern of crushed crystals of $V_{0.976}Cr_{0.024}O_2$ was taken with a Hägg-Guinier camera using KCl as an internal standard. The weak reflections marked by an asterisk cannot be indexed on an orthorhombic cell with $a \approx b \approx \sqrt{2}\, a_R$ and $c \approx 2c_R$, as proposed by Villeneuve *et al.*[9] Also the clearly resolved doublet (620)-(023) cannot be indexed on an orthorhombic cell with $a \approx b \approx 2\sqrt{2}\, a_R$ and $c \approx 2c_R$. The refined monoclinic lattice parameters for the room-temperature phase of $V_{0.976}Cr_{0.024}O_2$ are

$a = 9.0664(7)$ Å, $b = 5.7970(5)$ Å,

$c = 4.5255(4)$ Å, $\beta = 91.88(1)°$.

It should be noted that although the true symmetry is monoclinic the angle between the monoclinic (201) and $(20\bar{1})$ is 90.1°, so that the powder pattern might be indexed on a false orthorhombic unit cell. In-

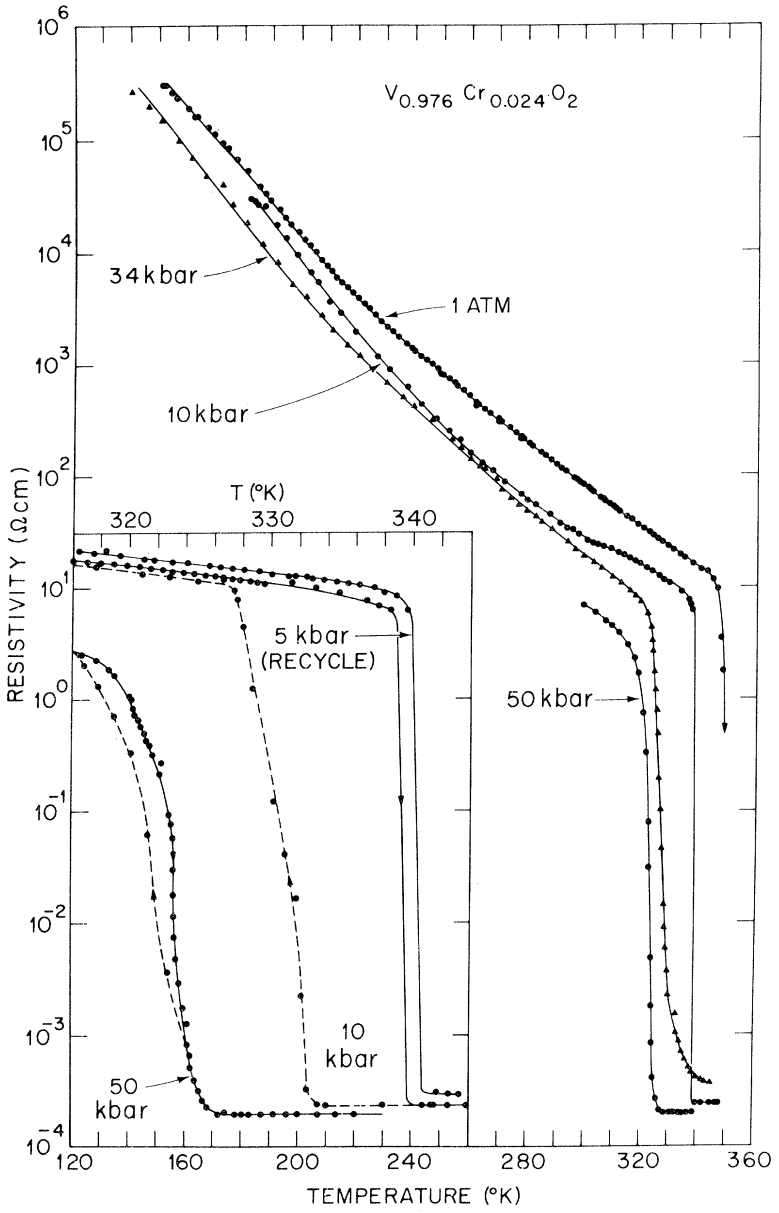

FIG. 5. Resistivity vs temperature at different pressures for a crystal of $V_{0.976}Cr_{0.024}O_2$. The insert shows (a) the change in sharpness and hystersis below and above the triple point and (b) the reversibility of the results. Triangles are for second sample.

deed, the single-crystal zero-layer precession photographs also appear orthorhombic, and the true symmetry was only revealed in the upper-layer photographs.

X-ray-intensity measurements of the three structures of $V_{0.976}Cr_{0.024}O_2$, R, M_2, and M_3, were taken automatically with a General Electric XRD-5 diffractometer. A scintillation counter and a decade scalar were used as the detection system. Single Zr-filtered Mo$K\alpha$ radiation was used with an 8° takeoff angle. For the two sets of data collected at (360 ± 5) and (180 ± 5) °K the temperature was maintained by blowing a stream of nitrogen gas directly on the crystal. The appropriate temperature and gas flow were controlled by the Varian temperature-control unit.

The 0.034-cm-diam sphere was oriented with $[010]_R$ parallel to the φ axis of the goniostat. The stationary-crystal–stationary-counter method for intensity-data collection was used with the background taken $\pm 2°$ off the peak maximum (2θ). We observed that the crystal, while going through the $M_2 \rightarrow R$ transition, did not coalesce from a twinned crystal to a single one at 360 °K. Precession photographs revealed that within a cone of ~30° about one of the $[110]_R$ the two individuals gave single diffraction spots. The intensity measurements were, therefore, limited to this cone within 10°–80°

TABLE I. Powder pattern of $V_{0.976}Cr_{0.024}O_2$ at 298 °K.

hkl	d_{obs}	d_{calc}	I_{obs}
$\bar{1}11$[a]	3.3470	4.3479	VW
$\bar{2}01$	3.2569	3.2548	M
201[b]	3.1465	3.1498	VS
310[a]	2.6789	2.6787	VW
021	2.4402	2.4404	M
400	2.2635	2.2654	
002		2.2615	VW
$\bar{2}21$	2.1636	2.1646	
$\bar{2}21$	2.1314	2.1328	W
$\bar{2}02$	2.0504	2.0505	W
202	1.9976	1.9975	VW
$\bar{1}30$[a]	1.8893	1.8898	VW
$\bar{3}12$[a]	1.7563	1.7534	VW
$\bar{4}21$	1.6749	1.6751	VW
222	1.6447	1.6447	M
330	1.6287	1.6277	M
402[b]	1.5732	1.5749	VW
$\bar{3}31$[a]	1.5405	1.5403	W
040	1.4493	1.4493	VW
$\bar{1}13$	1.4475	1.4478	W
601	1.4186	1.4186	W
620	1.3394	1.3394	W
023	1.3376	1.3376	W
$\bar{2}41$	1.3240	1.3239	W
241	1.3165	1.3166	VW
			VW

[a]Reflections not allowed in cell of Ref. 9; see text.
[b]Overlap reflection of KCl internal standard.

$= 2\theta$. A total of 71 independent reflections were used to refine the structure. A spherical absorption correction ($\mu R = 1.39$) was applied together with the Lorentz-polarization corrections. All refinements were carried out with the ORFLS program, using the scattering factors for neutral atoms[19] and the anomalous dispersion coefficients for Mo radiation.[20] The starting positional parameters were those for TiO_2.[21]

The M_2 structure was refined by using another sphere of 0.032-cm diam. This sphere was oriented with the $[010]_{M_2}$ parallel with the φ axis of the goniostat. The intensity measurements were collected automatically at 298 °K. Precession photographs showed that if the intensity measurements were restricted to a 2θ range of 35°–80°, a χ range 0°–60°, and $h = 0$, $h \geq 3$, one could clearly measure the intensities coming from one twin. These conditions resulted in a total of 457 independent reflections used in the refinements. The intensities were converted into structure factors by applying the spherical-absorption ($\mu R = 1.28$) and Lorentz-polarization corrections. The starting positional parameters were the transformed rutile ones.

The previous sphere was used to determine the structure of the M_3 phase at 180 °K. The same reflections observed for the M_2 phase were collected automatically. The identical procedure was applied to convert intensities to structure factors.

Tables II, III, and IV give the final positional and thermal parameters for $V_{0.976}Cr_{0.024}O_2$ at 360, 298, and 180 °K, respectively. The corresponding agreement R factors, $R = \sum |\Delta F| / \sum |F_0|$, were 0.029, 0.040, 0.050. Tables containing the observed and calculated structure factors for the three phases are omitted but are available on request. The interatomic distances and angles with their standard deviations, calculated by the ORFFE program, are reported in Tables V and VI. Figure 7 shows a projection of the M_2 structure on the (a, b) plane or the pseudorutile (a, c) plane. One rutile cell is outlined. In the rutile structure the oxygen octahedra are distorted such that there are four equivalent cation-oxygen distances in a plane and two equivalent distances perpendicular to this plane. The octahedra share edges along the c axis, forming infinite chains. These chains share vertices with the adjacent chains.

In the R phase of $V_{0.976}Cr_{0.024}O_2$ at 360 °K the two apical V-O distances are 1.933 Å and the four equatorial V-O distances are 1.920 Å. The average V-O distance is 1.927 Å, which gives an effective ionic radius of 0.57 Å for the six-coordinated cation. An index of distortion for the oxygen octahedron can be given as the ratio (apical V-O)/(equatorial V-O). For this phase the ratio is 1.007 while for the recently refined TiO_2 and CrO_2 it is[21] 1.016 and 0.990,[22] respectively. In the rutile structure each cation has ten nearest cation neighbors. Two of these neighbors lie along the c axis across the shared octahedral edge, with the remaining eight lying along the body diagonals across shared vertices. The V-V distance across the shared edge is 2.854 Å. This distance for TiO_2 is 2.958 Å and 2.916 Å for CrO_2.

One can see from Fig. 7 that the M_2 structure consists of four distorted rutile cells. There are two vanadium sites. V(1) moves out of the center of the oxygen octahedron in such a way that four of the six V-O distances decrease to an average value of 1.862 Å while two expand to 2.089 Å, the over-

TABLE II. Positional and thermal parameters of $V_{0.976}Cr_{0.024}O_2$ in the rutile structure at 360 °K.

	x	y	z	β_{11}	β_{22}	β_{33}	β_{12}	β_{13}	β_{23}
V	0.0	0.0	0.0	0.0110(4)	0.0110(4)	0.025(1)	0.0010(2)	0.0	0.0
O	0.3004(4)	0.3004(4)	0.0	0.0085(5)	0.0085(5)	0.019(1)	−0.0001(3)	0.0	0.0

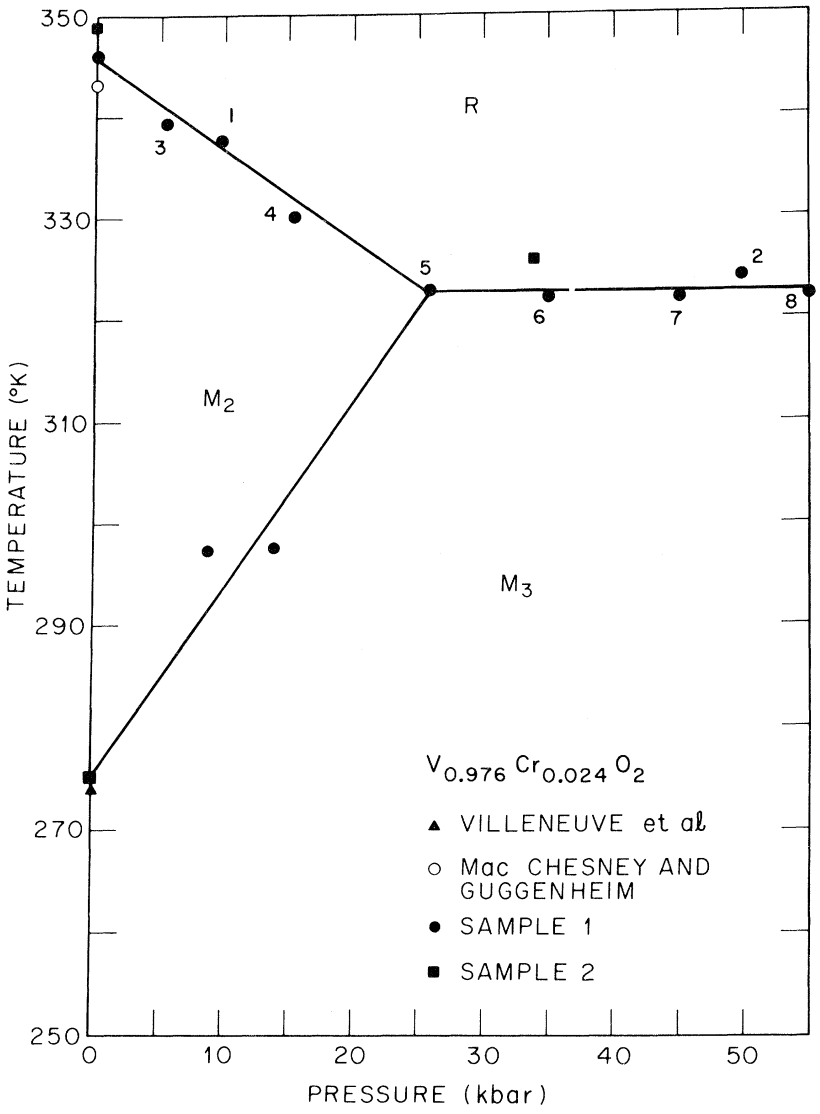

FIG. 6. Tentative temperature-pressure phase diagram for $V_{0.976}Cr_{0.024}O_2$. The numbers show the sequence in which the data points were obtained. The results are clearly reversible. The assignment of the M_2-M_3 boundary and the triple point is discussed in the text.

all average being 1.938 Å. The oxygen octahedron about V(2) distorts in a different fashion. The four equatorial V-O distances remain relatively constant, whereas the apical distances expand to 2.127 Å and contract to 1.726 Å, respectively. The average V(2)-O distance is 1.944 Å, and the over-all V-O distance in this structure is 1.941. For pure VO_2 in the M_1 phase the average V-O distance is 1.937 Å.[22] It seems that the addition of Cr to VO_2 does not have a significant effect on the V-O bond length.

The V(1) chains along the b_{M_2} or the pseudorutile c axis are comprised of alternating short and long V-V distances. They are 2.538 and 3.259 Å, respectively, the average being 2.899 Å. This value is 1.5% larger than the corresponding distance in the R structure at 360 °K. The V(2) chains are comprised of only one V-V distance (2.933 Å), which is 2.8% longer than the V(1)-V(1) average.

TABLE III. Positional and thermal parameters for M_2 phase of $V_{0.976}Cr_{0.024}O_2$ at 298 °K.

	x	y	z	β_{11}	β_{22}	β_{33}	β_{12}	β_{13}	β_{23}
V(1)	0.0	0.7189(1)	0.0	0.00124(6)	0.0038(2)	0.0052(2)	0.0	0.00066(7)	0.0
V(2)	0.2314(1)	0.0	0.5312(1)	0.00095(6)	0.0038(2)	0.0042(2)	0.0	0.00017(6)	0.0
O(1)	0.1482(2)	0.2475(4)	0.2942(4)	0.0015(2)	0.0014(5)	0.0044(5)	−0.0001(2)	−0.0003(2)	0.0005(4)
O(2)	0.3969(3)	0.0	0.2089(6)	0.0014(2)	0.0017(8)	0.0054(8)	0.0	0.0008(3)	0.0
O(3)	0.1000(3)	0.0	0.7987(6)	0.0014(2)	0.0015(8)	0.0047(8)	0.0	0.0009(3)	0.0

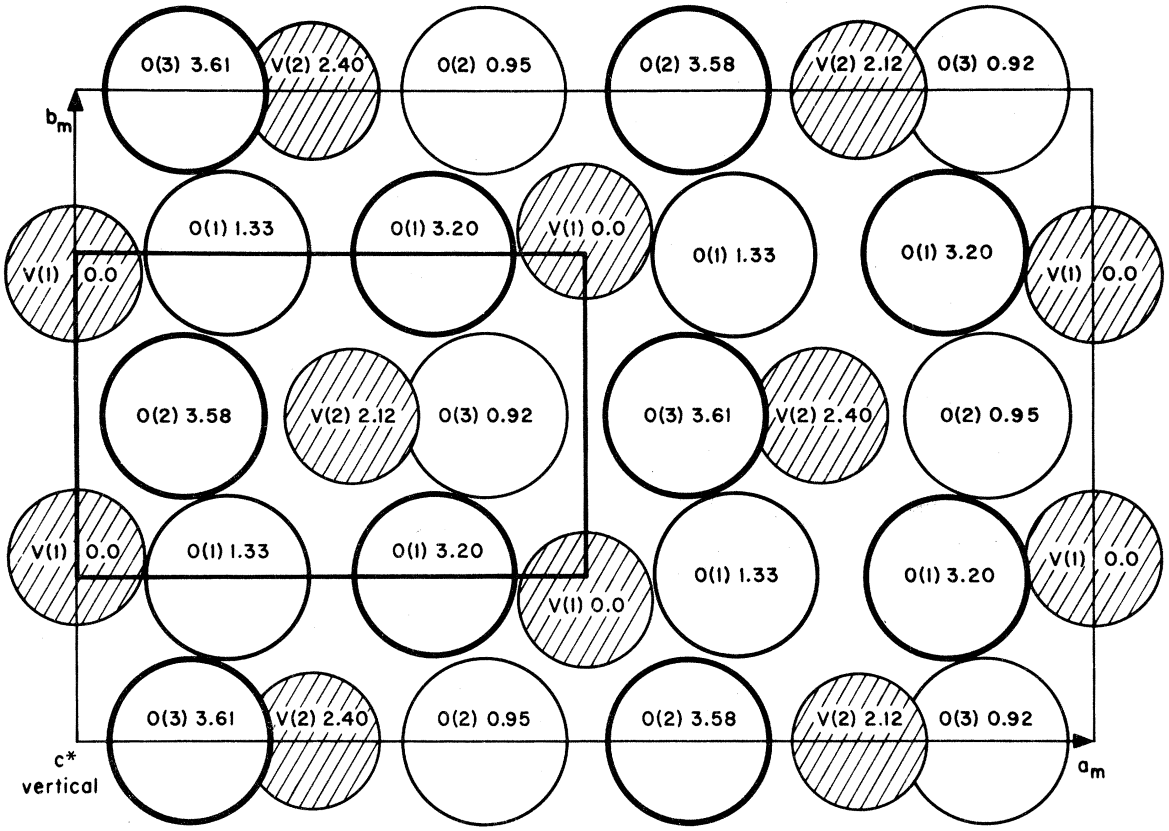

FIG. 7. Projection of the intermediate monoclinic phase (M_2) on the (a, b) plane or the pseudorutile (a, c) plane. The rutile cell is outlined for comparison.

Since the V(2) atoms have small displacements only in the $(x, z)_{M_2}$ plane, this results in a zig-zag pattern along the b_{M_2} axis. In pure VO_2 with the M_1 structure there is only one type of vanadium atom. The chains of nearest-neighbor vanadium atoms have both types of displacement, namely, an alteration in the interatomic distances and a zig-zag pattern along the pseudorutile c axis. The short distance is 2.613 Å and the long one is 3.176 Å.[23] The shortest V-V distance in the M_2 structure is 3.1% smaller than the shortest V-V distance in the M_1 structure.

In the M_3 structure at 180 °K the oxygen octahedra about V(1) and V(2) become slightly less distorted than their M_2 counterparts. For instance, in the V(1) octahedron the two longer distances decrease from 2.089 to 2.068 Å. In the V(2) octahedron the apical distances change from 2.127 and 1.726 to 2.105 and 1.751 Å, respectively. The V(1)-O and V(2)-O average distances are 1.929 and 1.946 Å with an over-all coverage of 1.938 Å. The short V(1)-V(1) distance remains constant within one standard deviation between M_2 at 298 °K

TABLE IV. Positional and thermal parameters for M_3 phase of $V_{0.976}Cr_{0.024}O_2$ at 180 °K.

	x	y	z	B (Å^2)
V(1)	0.0	0.7202(2)	0.0	0.55(3)
V(2)	0.2323(1)	0.0	0.5268(3)	0.46(3)
O(1)	0.1476(3)	0.2473(7)	0.2927(7	0.34(5)
O(2)	0.3966(5)	0.0	0.2068(10)	0.37(6)
O(3)	0.0992(5)	0.0	0.8001(10)	0.32(6)

TABLE V. Interatomic distances and angles in the rutile phase at 360 °K.

V − O×2	(1.933 ± 0.001) Å
V − O×4	(1.920 ± 0.001) Å
O − O×2	(2.854 ± 0.001) Å
O − O×2	(2.569 ± 0.001) Å
O − O×8	(2.725 ± 0.001) Å
O − V − O×2	(83.99 ± 0.06)°
O − V − O×2	(96.01 ± 0.06)°
O − V − O×8	90° (required by symmetry)
V − V across edge	(2.854 ± 0.001) Å
V − V across corner	(3.520 ± 0.001) Å

TABLE VI. Interatomic distances and angles in the M_2 and M_3 structures.

	V(1)—Octahedron	
	298 °K	180 °K
V(1) − O(1) × 2	(1.870 ± 0.002) Å	(1.869 ± 0.003) Å
V(1) − O(2) × 2	(1.854 ± 0.002) Å	(1.849 ± 0.003) Å
V(1) − O(3) × 2	(2.098 ± 0.002) Å	(2.068 ± 0.003) Å
O(1) − O(2) × 2	(2.725 ± 0.003) Å	(2.728 ± 0.005) Å
O(1) − O(3) × 2	(2.690 ± 0.003) Å	(2.683 ± 0.005) Å
O(2) − O(3) × 2	(2.899 ± 0.001) Å	(2.885 ± 0.001) Å
O(1) − O(2) × 2	(2.726 ± 0.003) Å	(2.709 ± 0.005) Å
O(1) − O(3) × 2	(2.686 ± 0.003) Å	(2.670 ± 0.005) Å
O(2) − O(2)	(2.703 ± 0.005) Å	(2.686 ± 0.009) Å
O(3) − O(3)	(2.613 ± 0.005) Å	(2.587 ± 0.009) Å
O(1) − V(1) − O(2) × 2	(94.13 ± 0.09)°	(93.5 ± 0.2)°
O(1) − V(1) − O(2) × 2	(94.06 ± 0.09)°	(94.4 ± 0.2)°
O(1) − V(1) − O(3) × 2	(85.42 ± 0.09)°	(85.8 ± 0.2)°
O(1) − V(1) − O(3) × 2	(85.26 ± 0.09)°	(85.3 ± 0.2)°
O(2) − V(1) − (3) × 2	(94.48 ± 0.08)°	(94.7 ± 0.1)°
O(2) − V(1) − O(2)	(93.6 ± 0.1)°	(93.2 ± 0.2)°
O(3) − V(1) − O(3)	(77.4 ± 0.1)°	(77.4 ± 0.2)°
	V(2)—Octahedron	
V(2) − O(1) × 2	(1.930 ± 0.002) Å	(1.925 ± 0.004) Å
V(2) − O(1) × 2	(1.975 ± 0.002) Å	(1.984 ± 0.004) Å
V(2) − O(2)	(2.127 ± 0.003) Å	(2.105 ± 0.004) Å
V(2) − O(3)	(1.726 ± 0.003) Å	(1.751 ± 0.005) Å
V(1) − O(1) × 2	(2.580 ± 0.003) Å	(2.606 ± 0.006) Å
O(1) − O(1)	(2.928 ± 0.005) Å	(2.916 ± 0.008) Å
O(1) − O(1)	(2.869 ± 0.005) Å	(2.853 ± 0.008) Å
O(1) − O(2) × 2	(2.711 ± 0.003) Å	(2.712 ± 0.005) Å
O(1) − O(2) × 2	(2.725 ± 0.003) Å	(2.729 ± 0.004) Å
O(1) − O(3) × 2	(2.743 ± 0.003) Å	(2.745 ± 0.005) Å
O(1) − O(3) × 2	(2.756 ± 0.003) Å	(2.765 ± 0.005) Å
O(1) − V(2) − O(2) × 2	(83.72 ± 0.07)°	(84.5 ± 0.1)°
O(1) − V(2) − O(2) × 2	(83.18 ± 0.07)°	(83.7 ± 0.1)°
O(1) − V(2) − O(2) × 2	(96.01 ± 0.07)°	(95.3 ± 0.1)°
O(1) − V(2) − O(2) × 2	(97.09 ± 0.07)°	(96.5 ± 0.1)°
O(1) − V(2) − O(1) × 2	(82.66 ± 0.07)°	(83.6 ± 0.1)°
O(1) − V(2) − O(1)	(96.5 ± 0.1)°	(94.6 ± 0.2)°
O(1) − V(2) − O(1)	(96.0 ± 0.1)°	(95.7 ± 0.2)°
	V − V distances	
	298 °K	180 °K
V(1) − V(1)	(2.538 ± 0.001) Å	(2.541 ± 0.003) Å
V(1) − V(1)	(3.259 ± 0.001) Å	(3.228 ± 0.003) Å
V(2) − V(2)	(2.933 ± 0.001) Å	(2.913 ± 0.001) Å
V(1) − V(2)	(3.421 ± 0.001) Å	(3.440 ± 0.001) Å
V(1) − V(2)	(3.536 ± 0.001) Å	(3.531 ± 0.001) Å
V(1) − V(2)	(3.442 ± 0.001) Å	(3.446 ± 0.001) Å
V(1) − V(2)	(3.702 ± 0.001) Å	(3.675 ± 0.001) Å

and M_3 at 180° K. The other V(1)-V(1) distance and the V(2)-V(2) one decrease from 3.259 and 2.933 to 3.228 and 2.913 Å, respectively.

V. DISCUSSION

The metal-insulator transition in VO_2 is not well understood. No conclusive evidence has been presented to show that the transition is driven by electronic effects[6] or lattice effects.[2,9,24] The present results indicate that the simple model of pairing vanadium atoms in the insulating phase, in order to account for the absence of long-range magnetic order, is not adequate. In Fig. 8 the positions of the vanadium atoms in each structure are compared. In the M_1 phase it has been suggested that vanadium-pair bonds are formed across the octahedral edges using the d orbital of symmetry xy (where x and y are axes pointing toward the two oxygens). The twisting of the bond may be related to mixing with the orbital $(x \pm y)z$ of π-like symmetry. This model would account for the lack of localized magnetic moments and long-range magnetic order in the insulating phase of $VO_2(M_1)$.[5,25] In M_2, half of the vanadium atoms pair but do not twist as in M_1. In contrast, the other half of the vanadium atoms twist but remain equidistant along the resulting zig-zag chain. It is difficult to rationalize the model for $VO_2(M_1)$ with the M_2 phase, as only half of the vanadium atoms are paired. Even in the low-temperature M_3 phase there is no increase in pairing but an over-all decrease in the V-V distance in the zig-zag chain. Anderson has suggested that a partial disproportionation of the vanadium d electrons might be possible.[26] Both the xy (σ-like) and the $(x+y)z$(π-like) orbitals might

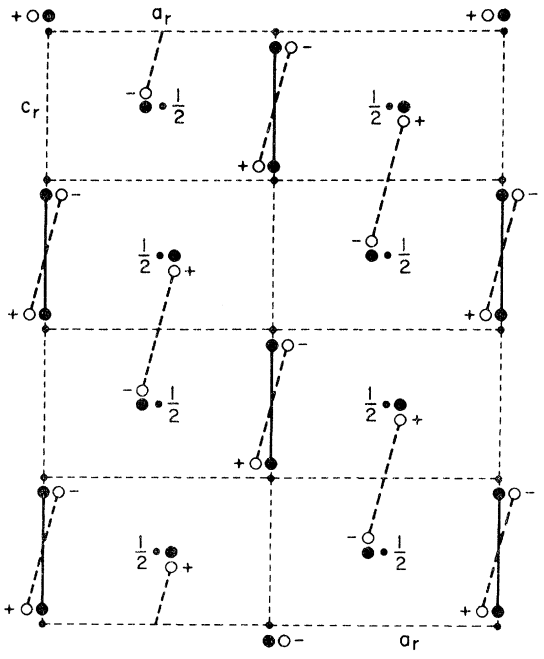

FIG. 8. Comparison of V-V pairing in the three phases (R, M_1, and M_2). In M_1 (open circles) all the vanadium atoms both pair and twist from the rutile positions. In M_2 (filled circles) half of the vanadium atoms pair but do not twist and the other half form unpaired zig-zag chains. (The distortions are exaggerated by a factor of 2 for clarity.)

be partially occupied in the paired vanadium atoms. The remaining vanadium atoms in the equally spaced zig-zag chain would then have less than one d electron. Crystal chemical arguments would rule out a complete disproportionation to the 3+ and 5+ configuration found in the compound $CrVO_4$, but without microscopic experimental evidence it is not clear if this idea would account for the properties of the insulating M_2 and M_3 phases.

The distortion of the octahedra is less in M_3 than in M_2. For instance, if one defines an index of distortion of the vanadium octahedra as the standard deviation of the observed V-O distances from the observed average, this index increases from 4.4×10^{-2} to 4.7×10^{-2} for V(1) and from 4.7×10^{-2} to 5.2×10^{-2} for V(2) on going from the M_3 to the M_2 structure. This decrease of the displacement of the V atom from the center of the octahedron with decreasing temperature argues against viewing the distortion from rutile to M_2 phase as a ferroelectric displacement of some type.[27]

ACKNOWLEDGMENTS

We thank P. W. Anderson, W. F. Brinkman, and T. M. Rice for many helpful discussions, and we thank J. B. MacChesney and H. J. Guggenheim for providing the crystals of $V_{0.976}Cr_{0.024}O_2$. We thank A. S. Cooper, E. M. Kelly, A. L. Stevens, and J. V. Waszczak for technical assistance. We are also grateful to A. Santoro of the National Bureau of Standards for helping us solve the twinning problem in $V_{0.976}Cr_{0.024}O_2$.

[1]D. B. McWhan, A. Menth, and J. P. Remeika, J. Phys. C 32, 1079 (1970), and references therein.
[2]W. Paul, Mat. Res. Bull. 5, 691 (1970).
[3]D. B. McWhan, T. M. Rice, and J. P. Remeika, Phys. Rev. Letters 23, 1384 (1969).
[4]D. B. McWhan, W. F. Brinkman, J. P. Remeika, J. P. Maita, T. M. Rice, and A. Menth, Phys. Rev. Letters 27, 941 (1971).
[5]Mats Israelsson and Lars Kihlborg, Mat. Res. Bull. 5, 19 (1970).
[6]T. M. Rice, D. B. McWhan, and W. F. Brinkman, in *Proceedings of the Tenth International Conference on the Physics of Semiconductors, Boston* 1970, edited by S. P. Keller, J. C. Hensel, and F. Stein (AEC, Washington, D. C., 1971), p. 6293.
[7]J. Galy, A. Casalot, J. Daniel, and P. Hagenmuller, Bull. Soc. Chim. France 1, 227 (1967).
[8]T. Mitsuishi, Japan. J. Appl. Phys. 6, 1060 (1967).
[9]G. Velleneuve, A. Bordet, A. Casalot, and P. Hagenmuller, Mat. Res. Bull. 6, 119 (1971).
[10]J. B. MacChesney and H. J. Guggenheim, J. Phys. Chem. Solids 30, 225 (1969).
[11]G. Anderson, Acta Chem. Scand. 8, 1599 (1954).
[12]M. Marezio, P. D. Dernier, D. B. McWhan, and J. P. Remeika, Mat. Res. Bull. 5, 1015 (1970).
[13]J. M. Honig and T. B. Reed, Phys. Rev. 174, 1020 (1968), and references therein.
[14]D. N. Lyon, D. B. McWhan, and A. L. Stevens, Rev. Sci. Instr. 38, 1234 (1967).
[15]D. B. McWhan, T. M. Rice, and P. H. Schmidt, Phys. Rev. 177, 1063 (1969).
[16]C. N. Berglund and A. Jayaraman, Phys. Rev. 185, 1034 (1969).
[17]L. Ladd and W. Paul, Solid State Commun. 7, 425 (1969).
[18]E. Ryder, quoted in Ref. 16.
[19]D. T. Cromer and J. T. Waber, Acta Cryst. 18, 104 (1965).
[20]D. T. Cromer, Acta Cryst. 18, 17 (1965).
[21]S. C. Abrahams and J. L. Bernstein, J. Chem. Phys. 55, 3206 (1971).
[22]P. Porta, M. Marezio, J. P. Remeika, and P. D. Dernier, Mat. Res. Bull. 7, 157 (1972).
[23]J. M. Longo and P. Kierkegaard, Acta Chem. Scand. 24, 420 (1970).
[24]C. N. Berglund and H. J. Guggenheim, Phys. Rev. 185, 1029 (1969).
[25]J. B. Goodenough, *Magnetism and the Chemical Bond* (Interscience, New York, 1963).
[26]P. W. Anderson (private communication).
[27]J. B. Goodenough, quoted in Ref. 9.